Refinement of Eutectic Si Phase in Al-5Si Alloys with Yb Additions

J.H. LI, S. SUETSUGU, Y. TSUNEKAWA, and P. SCHUMACHER

A series of Al-5 wt pct Si alloys with Yb additions (up to 6100 ppm) have been investigated using thermal analysis and multiscale microstructure characterization techniques. The addition of Yb was found to cause no modification effect to a fibrous morphology involving Si twinning; however, a refined plate-like eutectic structure was observed. The Al_2Si_2Yb phase was observed with Yb addition level of more than 1000 ppm. Within the eutectic Al and Si phases, the Al_2Si_2Yb phase was also found as a precipitation from the remained liquid. No Yb was detected in the α-Al matrix or plate-like Si particle, even with Yb addition up to 6100 ppm. The absence of Yb inside the eutectic Si particle may partly explain why no significant Si twinning was observed along $\{111\}_{Si}$ planes in the eutectic Si particle. In addition, the formation of the thermodynamic stable YbP phases is also proposed to deteriorate the potency of AlP phase in Al alloys. This investigation highlights to distinguish the modification associated with the ever present P in Al alloys. We define modification as a transition from faceted to fibrous morphology, while a reduction of the Si size is termed refinement.

DOI: 10.1007/s11661-012-1410-3

I. INTRODUCTION

AL-SI-BASED alloys, *i.e.*, A356, are dominant for the foundry application which constitutes the majority of all castings. The size and shape of eutectic Si in hypoeutectic Al-Si alloys and primary Si in hypereutectic Al-Si alloys have a key influence on the final mechanical properties of the manufactured parts. The modification of the Si morphology from flake-like to fibrous form greatly improves the mechanical properties. Therefore, the modification of eutectic Si in Al-Si alloys has been widely investigated in the field of solidification since the first modification phenomenon was discovered by Pacz,[1] where an Al-15 wt pct Si alloy was stirred in a sodium fluoride flux and a remarkable increase in the mechanical properties was achieved.

The modification of the eutectic Si in hypoeutectic Al-Si alloys is normally achieved in two different ways: by addition of certain modified elements (chemical modification)[2–13] or by rapid solidification (quench modification),[13] although ultrasonic vibration[14] and electromagnetic field[15] were also reported to refine the eutectic Si. With respect to chemical modification, several common modifying elements, *i.e.*, Sr and Na, have been widely investigated over the years and are widely used in the casting industry to modify the Si morphology from flake-like to fine fibrous. However, the exact mechanism involved behind this process is still under debate. Even for the earliest discovered element Na, several mechanisms still coexist. For example, the addition of Na into the Al-Si alloys was proposed to cause the obstruction of Si crystal growth by surface adsorption,[16] although Si crystal growth was also postulated to be hindered *via* the presence of sodium-rich $NaAlSi_{1.25}$ or $NaAlSi_{1.33}$ compounds.[17] In contrast, the addition of Na was also reported to retard the nucleation of Si by adsorption on the nuclei interface, during eutectic solidification.[18] Another modification mechanism, proposed by Guillet[19,20] suggests that the addition of Na poisons the Al_2O_3 and SiO_2 impurity particles, which could act as heterogeneous nucleation sites. It was demonstrated by Flood and Hunt[21] using quench experiments that the addition of Na not only changed the growth morphology but also prevented nucleation ahead of the eutectic growth front, so that a higher undercooling and finer eutectic lammelar spacing can be achieved. It should be noted that the higher undercooling obtained in Reference 21 can be attributed to the poisoning of AlP phase, which is ever present in Al alloys, even with high-purity Al materials. This poisoning can be caused by the formation of Na_3P,[22] depleting AlP phase. With respect to quench modification, our recent melt-spun experiments[13,23] clearly reveal that nanoscale-twinned Si particles were formed directly from the liquid in Al-5 wt pct Si alloys with and without trace-modified elements (Sr and P) during rapid quenching. The addition of Sr (100 ppm) into Al-5Si-based alloys was found to promote the twinning of Si particles on the grain boundary and the formation of Si precipitates in the α-Al matrix.

Although the modification mechanism is still a matter of debate, in particular nucleation, it was generally accepted that nucleation and growth mainly control

J.H. LI, University Assistant at Chair of Casting Research, is with the Department of Metallurgy, University of Leoben, 8700 Leoben, Austria. Contact e-mail: jiehua.li@hotmail.com S. SUETSUGU, Master Student, and Y. TSUNEKAWA, Professor, are with Toyota Technological Institute, Hisakata 2-12-1, Tempaku, Nagoya, 468-8511, Japan. P. SCHUMACHER, Professor at Chair of Casting Research, is with the Department of Metallurgy, University of Leoben, and also Managing Director, with Austrian Foundry Research Institute (ÖGI), Parkstrasse 21, Leoben, Styria 8700, Austria.

Manuscript submitted January 2, 2012.
Article published online September 22, 2012

modification. The impurity-induced twinning (IIT) growth mechanism proposed by Lu and Hellawell[2] and twin-plane re-entrant edge growth mechanism (TPRE) proposed by Wanger[24] and Hamilton and Seidensticker[25] are to date the accepted models. TPRE growth mechanism proposed that growth occurred more readily at the re-entrant corners during modification of Ge crystals. IIT growth mechanism proposed that the impurities were adsorbed on the growing surfaces of Si and caused frequent twinning to occur. The geometrical, ideal radius ratio ($r_{modifier}/r_{Si}$) to cause IIT is about 1.646. Both IIT and TPRE mechanisms have been experimentally supported in the cases of Na,[16–22] Sr,[9] and Eu.[11] However, only in the cases of Sr and Na, twinning was observed by TEM under conventional casting condition with slow cooling rate. Eu and Sr have been observed to be present in the eutectic Si of Al-Si alloys using μ-XRF mapping,[10,11] STEM-EDX map and atom probe tomography,[9] respectively, although μ-XRF mapping reveals that Sr is homogenously distributed within the eutectic Si, while STEM-EDX map and atom probe tomography shows Sr is segregated at the re-entrant corners and growing plane. This difference may be due to the techniques and resolution used, however, the segregation of Sr and Eu into eutectic Si indeed causes a fine fibrous morphology. A similar observation using electron probe microanalysis technique (EPMA) also shows that Sr resides mostly inside the Si in A356 alloy.[12]

In contrast to Na, Sr, and Eu, Yb was not chemically detected to be present in the eutectic Si, but appeared to be precipitated independently in the vicinity to the Si phase.[11] This is remarkable as Yb has a suitable radius ratio of $r_{Yb}/r_{Si} = 1.646$ exactly fitting the IIT theory. Moreover, previous study[8] suggests that the modification ability of an element may be the result of a certain combination of the valence electron charge number, the atom number, and atomic radius of the modifier, also implying that Yb may be an effective modifier. However, to date, there are still only a limited number of detailed investigations on the effect of Yb addition on the eutectic Si phase in Al-Si alloys.[4,5,11] Particular pertinent questions that remain to be explored are (1) the distribution of Yb at the re-entrant edges/or corner of the Si crystal and (2) the effect of Yb on Si twinning. The main motivation of this study is to investigate the effect of Yb addition at different levels on the eutectic Si phase in Al-5 wt pct Si alloys, with a focus on the distribution of Yb within Si and its effect on Si twinning.

II. EXPERIMENTAL METHODS

A series of Al-5 wt pct Si alloys (wt pct, used throughout the article unless otherwise noted) with Yb additions (up to 6100 ppm) were prepared using a commercial purity Al (99.7), Al-12Si (containing 0.9 Fe, and 0.355 Mn) master alloy and Al-5Yb master alloy. For comparison, a high-purity Al-5Si-6100 ppm Yb alloy was also prepared using a high-purity Al (4N), Si (5N), and commercial purity Al-5Yb master alloy. The chemical concentration of Yb was determined by inductively coupled plasma atomic emission spectrum (ICP-AES) apparatus, while other elements are given as nominal composition in Table I.

The experimental alloys were melted in an electric resistance furnace, and the temperature of the melt was kept at 993 K (720 °C). The Al-5Yb master alloy was added before casting. Each addition level was performed into a single batch. No degassing was performed before casting. At least, two samples for each addition level were taken to perform thermal analysis using a quick-cup method. About 5 minutes after the addition of the Al-5Yb master alloy, thermal analysis was performed to elucidate the thermal kinetics during solidification.

Optical microscopy (OM), SEM, and TEM were employed to characterize the microstructure. Samples for the OM, SEM, and TEM observations were taken from the center parts at the vicinity of the thermal couple. The specimens for OM and SEM investigation were mechanically ground, polished, and then etched using a mixture of 13 g boric acid, 35 g HF, and 800 mL H_2O. The specimens for TEM investigation were mechanically ground, polished, and dimpled to about 30 μm, followed by ion-beam milling using a Gatan Precision Ion Polishing System (PIPS, Gatan model 691). Transmission electron microscopy (TEM) was performed using a Philips CM12 microscopy operated at 120 kV and an image-side Cs-corrected JEOL-2100F operated at 200 kV.

Further investigation on the solidification behavior was also performed by the Scheil simulation using Thermo-calc software with TTAL5 database, with the aim to predict the possible phases and their formation temperatures in the Al-5Si alloys with (Alloy A,

Table I. The Chemical Compositions of Al-5Si Alloys With and Without the Yb Addition (Wt Pct)

	Elements				
Alloys	Si	Fe	Mn	Yb (ppm)	Al
Alloy A	5.00	0.37	0.11	—	balance
Alloy B	5.00	0.37	0.11	50	balance
Alloy C	5.00	0.37	0.11	500	balance
Alloy D	5.00	0.37	0.11	1000	balance
Alloy E	5.00	0.37	0.11	2000	balance
Alloy F	5.00	0.37	0.11	6100	balance
Alloy G	5.00	—	—	6100	balance

commercial purity) and without (high purity) impurities. However, no similar simulation was performed for the other experimental alloys containing Yb (Alloys B to G) because of a lack of thermodynamic data.

III. RESULTS

A. *Thermal Analysis of Al-5Si Alloys With and Without Yb Additions*

Figure 1 shows some typical cooling curves taken from Al-5Si alloys with and without the Yb addition. It should be noted that, for clarity, these cooling curves were separated (*i.e.*, shifted by 100 s), respectively. The cooling rate during thermal analysis was evaluated to be about 22 K min^{-1}. The liquidus temperature of the Al-5Si-based alloy (Alloy A) was evaluated to be about 903 K (630 °C), as shown in Figure 1(b). With increasing Yb additions, the liquids of primary α-Al decreases (refer to the first peak of α-Al in Figure 1(d)). The decrease in the liquidus temperature with increasing Yb additions suggests that the ternary alloy behaves similar to the binary Al-Yb alloy. The eutectic arrest area is enlarged, as shown in Figure 1(c). The eutectic nucleation temperature (T_N), minimum temperature (T_{Min}), and growth temperature (T_G) were determined and are listed in Table II. For this purpose, the first derivative of the cooling curve was superimposed on the normal curve, as shown in Figure 1(d). The first derivative at each point represents the solidification rate of the alloy.

The nucleation temperature, T_N, is defined as the point where the first silicon crystals nucleate and start to grow releasing latent heat. This is manifested by a change of slope in the cooling curve. This change in slope can be seen more clearly on the first derivative of the cooling curve.[4] The minimum temperature, T_{Min}, is defined as the point where the newly nucleated crystals, together with aluminum in the eutectic proportions, have grown to such an extent that the latent heat, evolved during the growth process, balances the heat flow out of the system. This depends upon the cooling rate and heat capacity of the solidifying system. Furthermore, according to free growth model,[26] free growth from particles stops at the T_{Min} because the critical radius becomes larger than the radius of the remaining inactive heterogeneous sites because of reheating. After this point, recalescence occurs, during which the release of latent heat surmounts the heat extraction from the system, a new heat balance is obtained, which rightfully should be defined as the "steady-state growth temperature" of the eutectic reaction. Recalescence is the difference between the T_{Min} and T_G temperatures ($T_G - T_{Min}$).

The measured T_N of eutectic Si (*i.e.*, 847 K (574 °C) for Alloy A without Yb addition) is close to the predicted equilibrium eutectic temperature [847 K (574 °C)] using Thermo Calc Scheil simulation with TTAL5 database, as shown in Figure 2(b), suggesting little or no undercooling. However, it should be noted that the nucleation temperature, T_N, is affected by the nucleation conditions in the alloys. Thermo Calc simulation only gives some information in equilibrium or Scheil condition. Nevertheless, Thermo Calc Scheil simulation indicates that the impurity elements (Fe and Mn) depress the equilibrium eutectic temperature from 850 K to 847 K (577 °C to 574 °C), as shown in Figure 2(a). The predicted eutectic temperatures [850 K and 847 K (577 °C and 574 °C)] were defined to be the equilibrium eutectic temperature (T_{eq}) of high-purity Al-5Si alloy (Alloy G) and commercial purity Al-5Si alloys (Alloys A to F), respectively.

Up to 1000 ppm Yb addition, no appreciable change of the thermal kinetics during solidification was observed. With increasing Yb addition, the eutectic arrest was displaced to lower temperatures (T_{Min}), suggesting that Si was hindered to grow by the Yb addition. The eutectic growth temperature (T_G) was also displaced to lower temperatures (*i.e.*, 836.5 K (563.5 °C), with 2000 ppm Yb addition; and 833 K (560 °C), with 6100 ppm Yb addition). In the case of high-purity Al-5Si-6100 ppm Yb alloy (Alloy G), the eutectic growth temperature was also decreased to 835.3 K (562.3 °C). It is worth noting that an inflection was observed for commercial purity alloys (Alloys A to F), as marked with an arrow in Figure 1(d), while no similar inflection was observed for high-purity alloy (Alloy G), as shown in Figure 1(e). The formation of the inflection may be attributed to the impurity effects of Fe and Mn elements on nucleation and growth of eutectic Si, *i.e.*, the formation of β-Al_5FeSi phase, as predicted in Figure 2(b).

The nucleation undercooling ($T_{eq} - T_N$) of the eutectic arrest was determined. No significant undercooling [0 K (0 °C)] was observed in the Alloy A without Yb addition. Increasing Yb addition results in increasing undercooling, suggesting the depletion of possible nuclei (*i.e.*, AlP) poisoned by Yb addition. It should be noted that a disagreement was also observed in Alloy B and Alloy C, which may be because of experimental error; however, the whole tendency is consistent. A higher undercooling [18.2 K (18.2 °C)] was observed for high-purity Al-5Si-6100 ppm Yb alloy (Alloy G), much higher than 3.8 K (3.8 °C) for commercial purity Al-5Si-6100 ppm Yb alloy (Alloy F). This difference [14.4 K (14.4 °C)] can be attributed to even fewer nuclei (*i.e.*, AlP) in the high-purity Al-5Si-6100 ppm Yb alloy (Alloy G) which are poisoned by Yb addition. It should be noted that, in the case of high-purity Al-5Si-6100 ppm Yb alloy (Alloy G), the eutectic nucleation temperature [T_N, 831.8 K (558.8 °C)] is slightly lower than the eutectic growth temperature [T_G, 835.3 K (562.3 °C)].

The same tendency is also true with the recalescence ($T_G - T_{Min}$) and growth undercooling ($T_{eq} - T_G$). A low recalescence [1.1 K (1.1 °C)] and growth undercooling [8.4 K (8.4 °C)] were observed in the Alloy A without Yb addition. No significant difference was observed with the Yb addition (up to 1000 ppm). Increasing Yb addition (above 1000 ppm) results in increasing recalescence and growth undercooling. A relatively higher recalescence [5.8 K (5.8 °C)] and growth undercooling [14.7 K (14.7 °C)] were observed for high-purity Al-5Si-6100 ppm Yb alloy

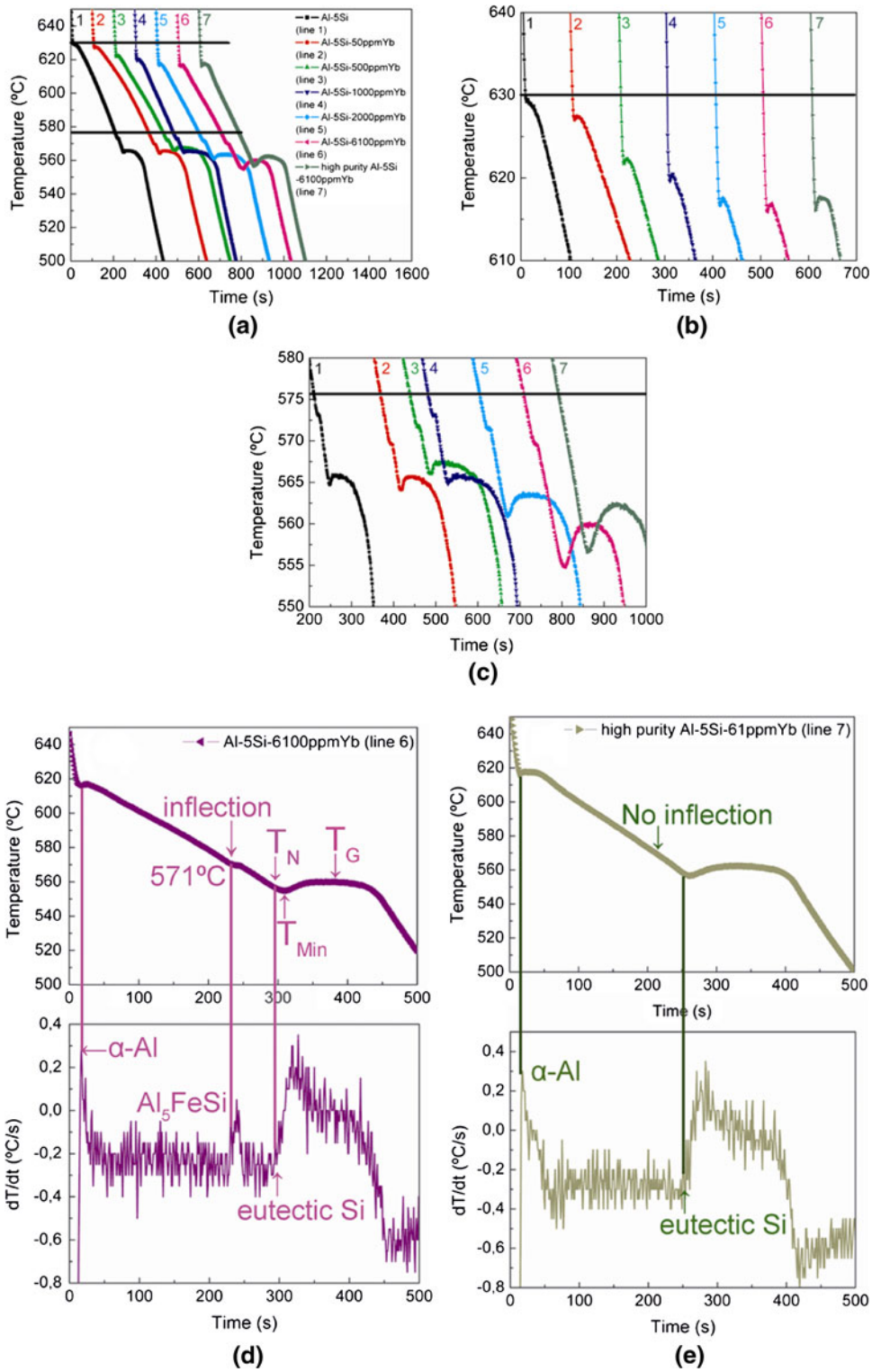

Fig. 1—Cooling curves (*a*) taken from Al-5Si alloys with and without Yb addition. The nucleation of α-Al is enlarged in (*b*). The eutectic arrest area is also enlarged in (*c*). Special focus is on Alloy F (Al-5Si-6100 ppm Yb, line 6) (*d*) and Alloy G (high-purity Al-5Si-6100 ppm Yb, line 7) (*e*). The main points (T_N, T_{Min}, T_G) are also marked in (d).

(Alloy G), slightly higher than 5.4 K and 14.0 K (5.4 °C and 14.0 °C) for commercial purity Al-5Si-6100 ppm Yb alloy (Alloy F). This difference [0.4 K and 0.7 K (0.4 °C and 0.7 °C)] can be also attributed to the fewer nuclei (*i.e.*, AlP), which almost require poisoning by Yb, in high-purity alloys. On the basis of these results, the

Table II. Nucleation Temperature (T_N), Minimum Temperature (T_{Min}), Growth Temperature (T_G), Nucleation Undercooling ($T_{eq} - T_N$), Growth Undercooling ($T_{eq} - T_G$), and Recalescence ($T_G - T_{Min}$) for Al-5Si Alloys With and Without the Yb Addition

Alloys	Yb (ppm)	T_N (K)	T_{Min} (K)	T_G (K)	Nucleation Undercooling $T_{eq} - T_N$ (K)	Growth Undercooling $T_{eq} - T_G$ (K)	Recalescence $T_G - T_{Min}$ (K)
Alloy A	—	847.0	837.5	838.6	0.0	8.4	1.1
Alloy B	50	847.1	837.7	839.4	0.9	7.6	1.7
Alloy C	500	847.5	839.0	840.4	0.5	6.6	1.4
Alloy D	1000	845.7	835.4	837.5	1.3	9.5	2.1
Alloy E	2000	844.1	833.8	836.5	2.9	10.5	2.7
Alloy F	6100	843.2	827.6	833.0	3.8	14.0	5.4
Alloy G	6100	831.8	829.5	835.3	18.2	14.7	5.8

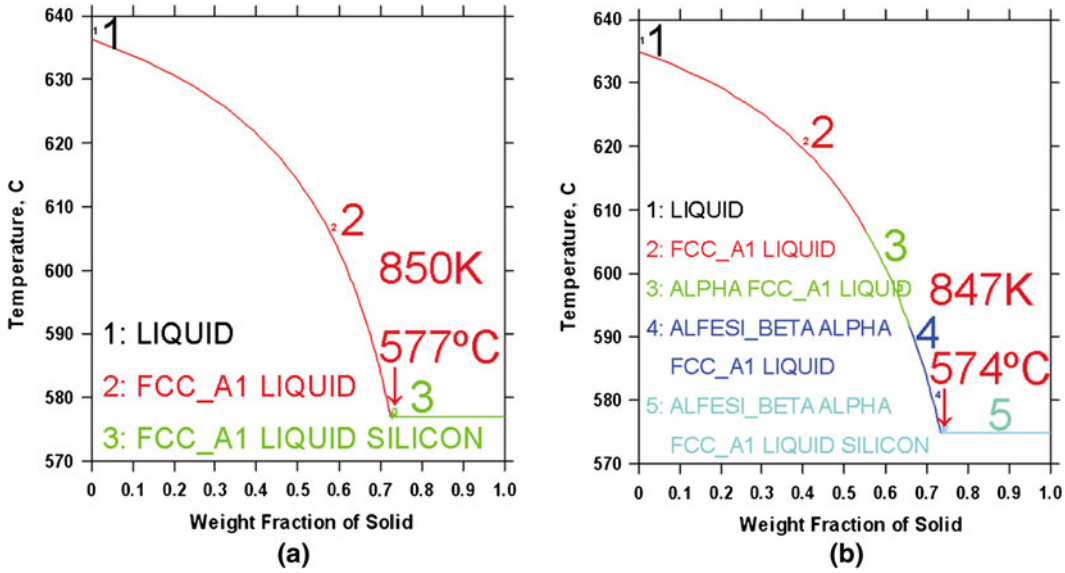

Fig. 2—Weight fraction of phases in commercial purity Al-5Si alloy without (*a*) and with (*b*) Fe (0.37) and Mn (0.11) impurities, simulated by using Scheil module with a database TTAL5.

samples with the additions of above 1000 ppm of Yb (Alloys D to G) were used for microstructure characterization.

B. *OM and SEM Observations of Al-5Si Alloys With and Without Yb Additions*

Figure 3 shows representative eutectic structures observed by OM at low magnifications. For comparison, a high-purity Al-5Si-200 ppm Na alloy is also shown in Figure 3(f). The eutectic Si in the alloy A without Yb addition is very coarse and flake-like, as shown in Figure 3(a). With the addition of up to 2000 ppm Yb (Figure 3(c)), the eutectic Si morphology remains unchanged, compared to the addition of 200 ppm Na. Up to 2000 ppm Yb, the eutectic Si is still plate-like, although a decrease in eutectic Si size was observed. A refined plate-like eutectic structure was achieved when the Yb content was increased to 6100 ppm (Figure 3(d)). It should be noted that, even in the case of 6100 ppm Yb addition, the eutectic structure is only refined in size, compared to the modification in shape and size of 200 ppm Na addition. The addition of high-purity elements (Alloy G, Figure 3(e)) causes a more refined plate-like eutectic structure and no significant β-Al_5FeSi phase. The more refined plate-like eutectic structure of high-purity alloy (Alloy G, Figure 3(e)) can be attributed to the relatively higher nucleation undercooling [18.2 K (18.2 °C)], growth undercooling [14.7 K (14.7 °C)], and recalescence [5.8 K (5.8 °C)] (Figure 1, Table II).

Overall distribution of Yb in the alloys can be easily observed by backscattered electron (BSE) image in SEM. The large atomic number difference makes compositional image possible, which gives rise to a brighter contrast of Yb-containing phases in BSE image mode. Figure 4 shows an Yb-containing phase observed in Al-5Si-1000 ppm Yb alloy. Similar Yb-containing phase was also observed above 1000 ppm Yb addition level (*i.e.*, 2000 ppm Yb (Alloy E) and 6100 ppm Yb (Alloys F and G)). At 500 ppm Yb, the Yb-containing phase was not observed, although it may also occur at this level. EDX analysis (Figure 4(b)) of the Yb-containing phase, as marked in Figure 4(a), indicates that the Yb-containing phase is the Al_2Si_2Yb phase. The Al_2Si_2Yb phase was also observed in high-purity Al-5Si-6100 ppm Yb alloy (Alloy G), although its size and amount are less evident. No Yb was detected in the α-Al matrix using EDX, even up to 6100 ppm Yb addition.

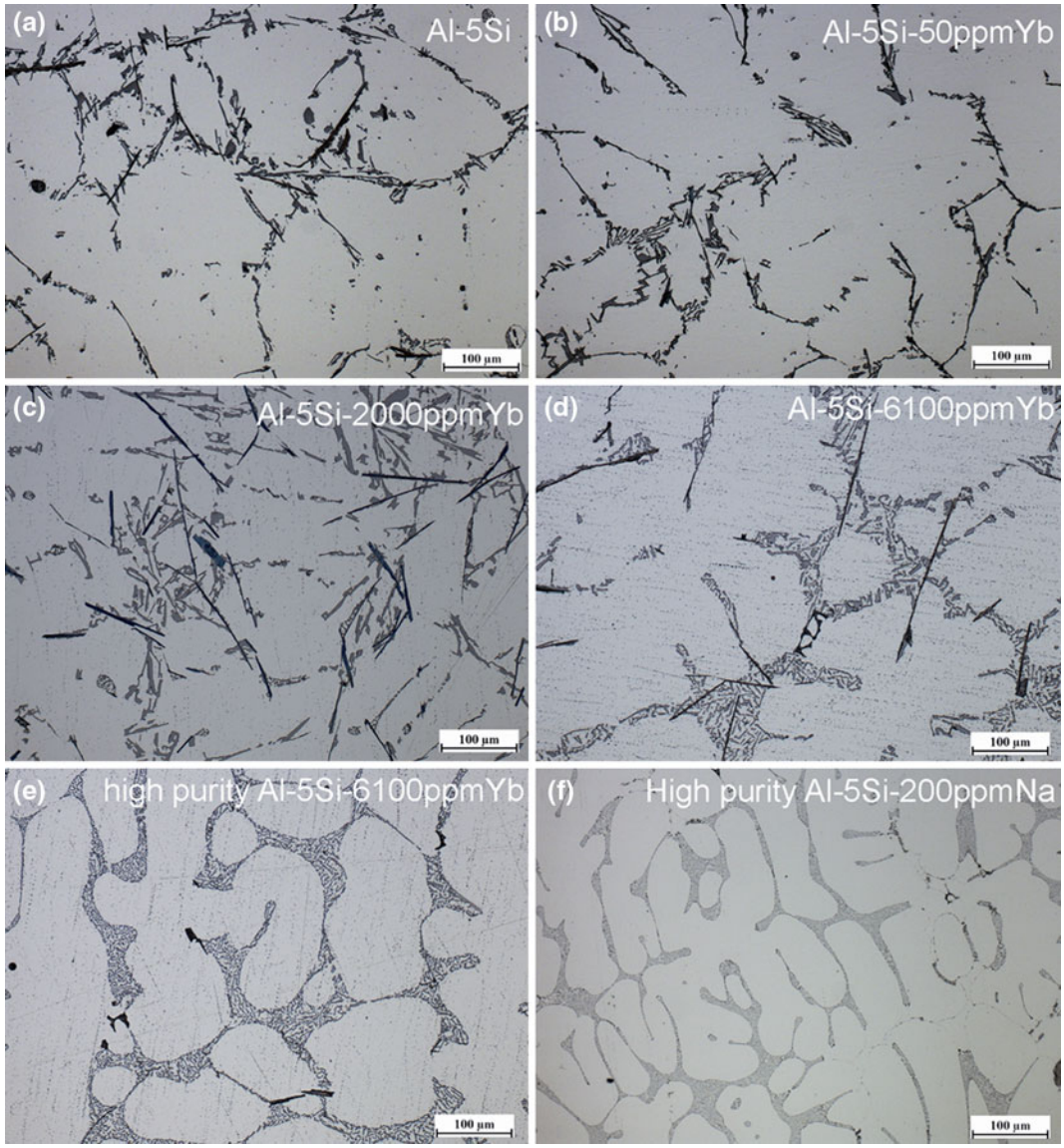

Fig. 3—Representative eutectic structures observed by optical microscopy at low magnifications. (*a*) Al-5Si alloy, (*b*) Al-5Si-50 ppm Yb alloy, (*c*) Al-5Si-2000 ppm Yb alloy, (*d*) Al-5Si-6100 ppm Yb alloy, and (*e*) high-purity Al-5Si-6100 ppm Yb alloy. For comparison, a high-purity Al-5Si-200 ppm Na alloy is also shown in (*f*).

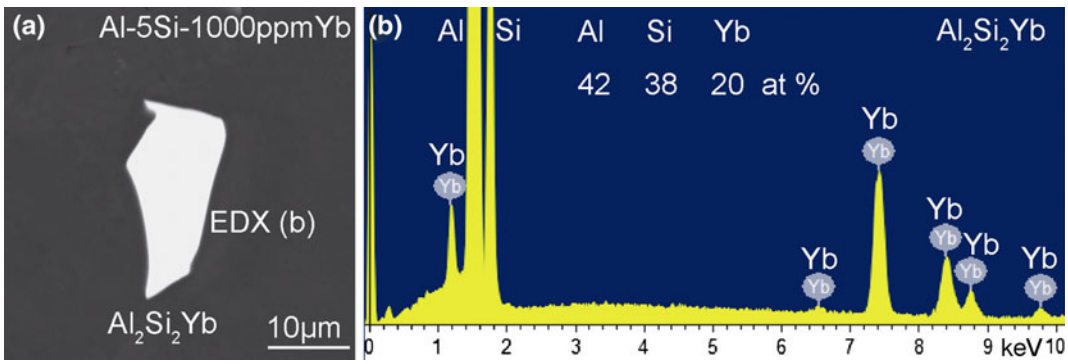

Fig. 4—Backscattered electron image (*a*) and EDX analysis (*b*) of the Al_2Si_2Yb phase in Al-5Si-1000 ppm Yb alloy.

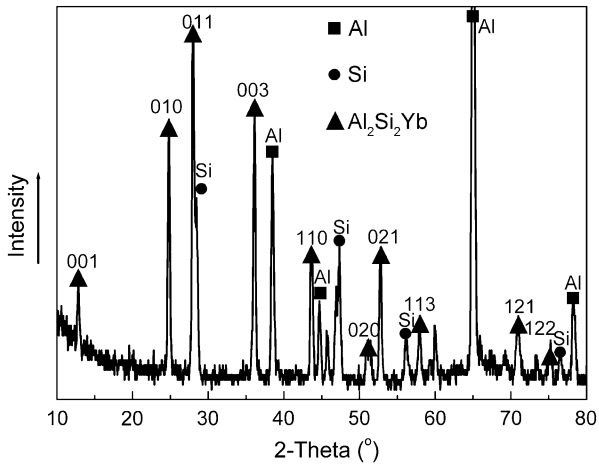

Fig. 5—XRD analysis to determine the lattice parameter of Al_2Si_2Yb phase in high-purity Al-5Si-3Yb alloy.

In order to determine the crystal structure and lattice parameter of Al_2Si_2Yb phase using XRD analysis, a high-purity Al-5Si-3Yb alloy was also prepared using the same method as for the other alloys. Backscattered electron (BSE) image and EDX analysis (not shown here) indicate that, even with higher amount of Yb addition, most of the observed intermetallic phases are still Al_2Si_2Yb. XRD result (Figure 5) shows there are some strong peaks obtained from the Al_2Si_2Yb phase. The crystal structure and lattice parameters of the Al_2Si_2Yb phase were determined to be hexagonal (a = 0.414482 nm, c = 0.68927 nm), which is in very close agreement with that in the previous article[27] using powder (hexagonal (a = 0.4144 nm, c = 0.6915 nm)) and that of the Al_2Si_2Sr phase (Hexagonal, a = 0.4187 nm, c = 0.7427 nm), although c (0.68927 nm) is a little smaller than that (0.7427 nm) of the Al_2Si_2Sr phase.

C. *TEM Observation of Commercial Purity Al-5Si-6100 ppm Yb Alloy*

Figure 6 shows a small refined faceted Si particle along the grain boundary in the commercial purity Al-5Si-6100 ppm Yb alloy. The Si particle was tilted to the principal twinning orientation of Si ($\langle 110 \rangle$) to observe twinning, as shown in Figure 6(b). Given that Si twinning may not be observed in every Si particle, at least, ten Si particles in three different TEM samples were observed; however, unexpectedly, no twinning was observed in the Si particle. Some surface artifact caused by sample preparation is present on Si particle (Figure 6(a)). Tilting the sample to another zone axis (*i.e.*, $\langle 110 \rangle_{Al}$, Figures 6(c) and (d)), again shows that no Si twinning has occurred.

Apart from the small refined faceted Si particle, most of eutectic Si appears to be plate-like. Figure 7 shows two plate-like Si phases appearing in the vicinity of a large plate-like β-Al_5FeSi phase. No high symmetry crystallographic orientation relationship was observed, indicating that the β-Al_5FeSi phase is not a nucleating site for Si. The β-Al_5FeSi phase was indexed using selected area diffraction pattern (SADP) and EDX analysis. Slow cooling rates, such as (22 K min^{-1}) observed here, promote the precipitation of β-Al_5FeSi phase. However, it should be pointed out that the effect of Fe addition on eutectic equilibrium temperature is relatively small, compared with the histrionically modifying elements (*i.e.*, Sr and Na).[28] It has to be proposed that the addition of Fe into Al-Si alloys does not change the eutectic Si from coarse and flake-like to fine and fibrous morphology.[23]

Figure 8 shows another plate-like eutectic Si in the commercial purity Al-5Si-6100 ppm Yb alloy. The width of the plate-like Si is about 0.4-0.5 μm. Some round artifacts on the surface of Si phase are present; however, these artifacts are believed to have formed during TEM sample preparation. A grain boundary of Si phase ($\{111\}_{Si}$) and α-Al matrix ($\{123\}_{Al}$) is highlighted in Figure 8(b). Clearly, the cube-to-cube orientation relationship between the Si particles within α-Al matrix, which was often observed in high-purity melt-spun Al-5Si alloy,[13,23] was not maintained at the grain boundary in this study. The TEM was set in nano-probe mode so that the investigated section was in the order of the electron probe itself. EDX analysis (Figure 8(c)) taken from the Si particle using a nanobeam (the beam size is about 1 nm) shows that only Si and Fe are present, while, Yb is not present. This indicates that Yb atoms do not concentrate in the eutectic Si, although Yb is present within the eutectic, *e.g.*, as Al_2Si_2Yb (Figure 4).

An interesting question arises: where is the Yb located? Apart from the formation of large Al_2Si_2Yb phase (Figure 4), some small Yb-containing precipitates were also observed in Al-Si eutectic in the commercial purity Al-5Si-6100 ppm Yb alloy, as shown in Figure 9(a). EDX analysis (Figure 9(c)) suggests that the small Yb-containing precipitate is also in the Al_2Si_2Yb phase. The presence of Cu peak is due to the TEM holder. It is worth noting that the corresponding SADP (Figure 9(b)) was taken using a large aperture containing α-Al matrix, two Si particles, and the Al_2Si_2Yb phase. However, no detailed structural information in terms of orientation relationship between the phases could be obtained, although it had been observed previously.[23]

IV. DISCUSSION

A. *Si Twinning*

No significant Si twins were observed in smaller refined, faceted Si particles (Figure 6) or larger plate-like eutectic Si (Figures 7 and 8) in the commercial purity Al-5Si-6100 ppm Yb alloy. This is in contrast to the interacted prediction of IIT and TPRE mechanism. Although it has been reported previously[2] that, in the case of chill cast, Yb addition results in an increase in twin density, compared with an unmodified alloy, it is of great importance to consider the features affecting the formation of Si twinning. One factor is the cooling rate. Higher cooling rates (*i.e.*, melt-spun Al-5Si alloys or chill cast) promote the Si twinning even without the

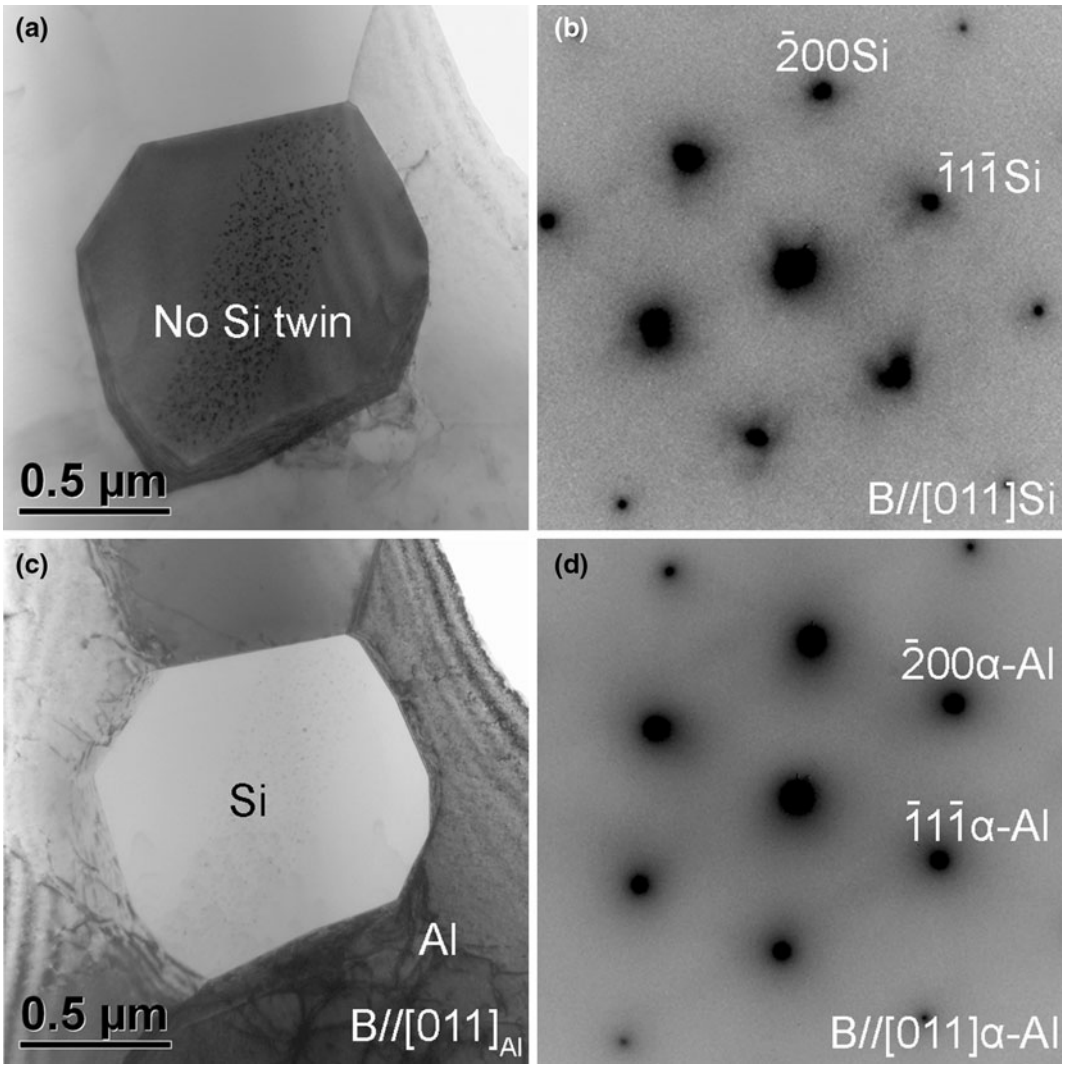

Fig. 6—TEM bright field images (*a*), (*c*), and the corresponding SADPs (*b*), (*d*) of the faceted Si phase on the grain boundary in commercial purity Al-5Si-6100 ppm Yb alloy. No clear Si twin was observed, although some surface artifact of oxidation on particles is present (a).

chemical addition of expected modifying agents.[13,23] Lower cooling rates (*i.e.*, for this study, thermal analysis, 22 K min^{-1} in a sand cast) reduce or lose the possibility of Si twinning by sufficient cooling. The other factor is the distribution of the modifying element. The Sr enrichment at the re-entrant edges/or corner of the eutectic Si promotes the twinning of Si particles.[9,10,23] It was also observed for the Eu addition.[11] This enrichment of Sr and Eu at the re-entrant edges/or corner of the eutectic Si may be attributed to their modification effects from flake-like to fibrous morphology. In contrast, Yb atoms do not concentrate in the eutectic Si (Figure 8) in the as-cast condition. Instead, they are likely to form the Al_2Si_2Yb phase (Figures 4 and 9) within the Al-Si eutectic. This observation is fully consistent with the μ-XRF mapping,[11] where Yb is not present in Si or Al but seems to be precipitated independently adjacent to the Si phase. The absence of Yb element inside the eutectic Si may partly explain why no significant Si twinning (Figure 6) was observed in the Alloy F with up to 6100 ppm Yb addition, even though Yb has a exactly suitable radius ratio (r_{Yb}/r_{Si} = 1.646) according to the IIT theory.

B. *The Formation of Al_2Si_2Yb or YbP Phase*

Yb was mainly consumed though the formation of Al_2Si_2Yb phases (Figures 4 and 9). It should be noted that the Al_2Si_2Yb phase identified in Al-Si-Yb-based alloy is very similar to the Al_2Si_2Sr phase observed in the Al-Si-Sr-based alloy.[13] Therefore, it can be expected that the formation of Al_2Si_2Yb phase deteriorates the effect of Yb additions on eutectic Si, if at all there is any. XRD analysis (Figure 5, Table III) also indicates that the crystallographic data of Al_2Si_2Yb phase (Hexagonal, a = 0.414482 nm, c = 0.68927 nm) is very close to that of Al_2Si_2Sr phase (Hexagonal, a = 0.4187 nm, c = 0.7427 nm). Thus, it can be expected that the Al_2Si_2Yb phase is not likely to be a nucleation site for eutectic Si in hypoeutectic Al-Si alloys.

It is generally accepted that the AlP phase is responsible for the Si nucleation both in hypo and hypereutectic Al-Si

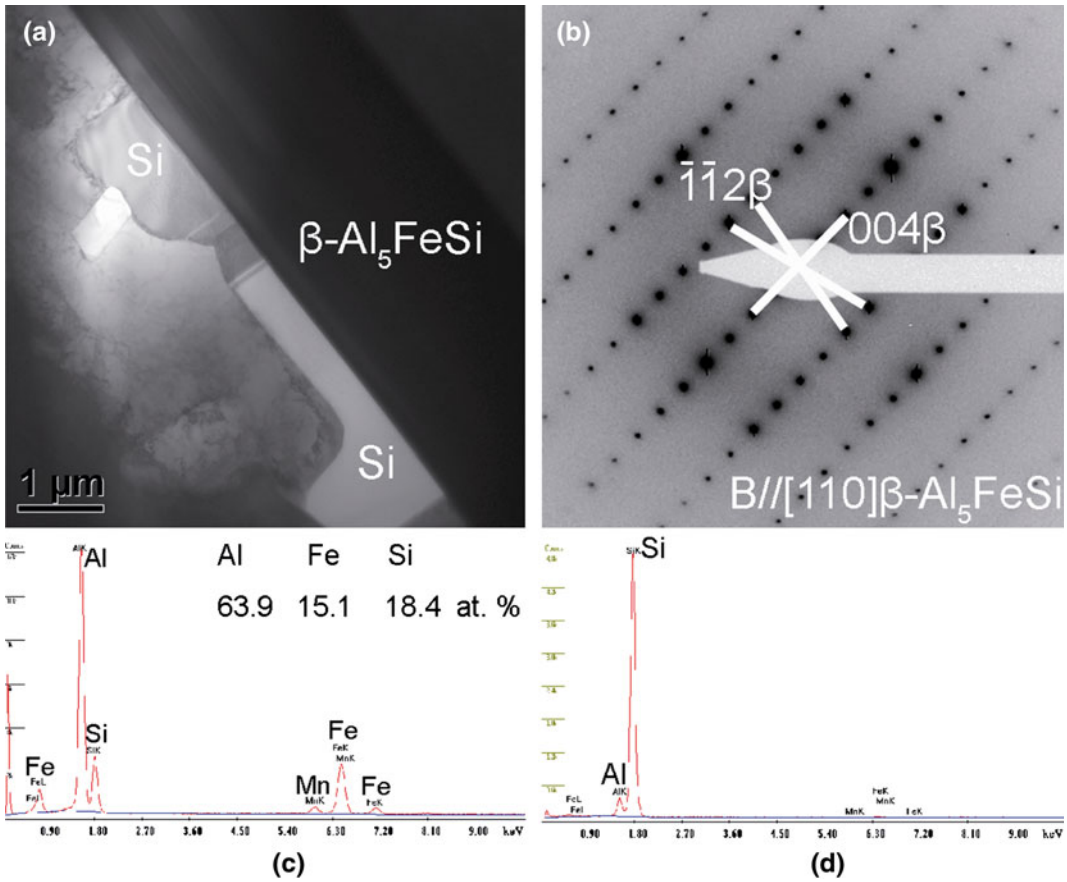

Fig. 7—TEM bright field image (*a*) and corresponding SADP (*b*), EDX analyses (*c*, *d*) of the plate-shaped Si phases in the vicinity of the β-Al_5FeSi phase in the commercial purity Al-5Si-6100 ppm Yb alloy.

alloys, as its crystal structure and lattice parameter have an excellent matching with Si (Table III). The lattice parameters for AlP and Si are 0.542 nm and 0.54306 nm, respectively, and corresponding structure types are B_3 and A4, respectively.[29] The disregistry between AlP and Si is only <1 pct.[30] Yb may be also partly consumed though the formation of YbP phase. Although the crystal structure and lattice parameter of YbP phase (Fm3m, NaCl, a = 0.5554 nm[31]) are very close to those of AlP, its potency for the Si nucleation is not experimentally supported, as shown here by the large observed nucleation undercooling (Table II).

Although there is a lack of strong experimental support to the existence of YbP phase in the current study considering the expected level of P (less than 20 ppm), the possible existence of YbP phase can be strongly supported in terms of thermodynamics (entropy, enthalpy, and Gibbs energy) of competing phosphide compounds (*i.e.*, Na_3P, Sr_3P_2, YP, and YbP). It has been reported that the entropy of YbP (5.76 J mol^{-1} K^{-1})[32] is much smaller than that of AlP (57.3 J mol^{-1} K^{-1}). Although the free enthalpy (ΔG, as documented by M. E. Schlesinger[33]) of YbP phase is not available, to our knowledge, it can be expected to be also much lower than that of AlP (−111.66 kJ.mol^{-1}), similar to YP, LaP, and ScP,[33,34] as listed in Table IV. It should be noted that the free enthalpy values (ΔG) of other phosphide compounds (*i.e.*, FeP, CrP, and MnP) are much closer to the value of AlP, which is consistent with the fact that these elements have no great influence on the nucleation of eutectic Si in Al-Si alloys. The thermodynamic consideration strongly supports that YbP phase is thermodynamically more stable and is highly likely to be preferentially formed, even with AlP acting as a nucleation site for Si. This also strongly supports the hypothesis that formation of the YbP phase will consume P and force the nucleation of Si to a higher undercooling, as observed in Table II.

The formation of the YbP phase is also consistent with the formation of other P-containing phases, *i.e.*, the formation of Na_3P[22] in the case of Na addition, and the formation of Sr_3P_2 compound in the case of Sr addition.[13,23] In both cases of Na and Sr, the estimated free enthalpy values of the formation of Na_3P and Sr_3P_2 (−635 and −134 kJ mol^{-1}, respectively) are much less than that of AlP phase (−111.66 kJ mol^{-1}).[33,34] The same hypothesis may be also true with the addition of Sc, La, Y, and Ca elements, having even more negative ΔG. With the presence of elements with a smaller enthalpy (ΔG), the AlP will deplete the nucleation sites for Si. The remaining amount of AlP will be determined by the competing phosphides which were only reported in some cases.[22]

A simplified formula has been presented by Ho and Cantor[22] to estimate the amount of Na required for forming Na_3P instead of AlP, assuming that AlP is

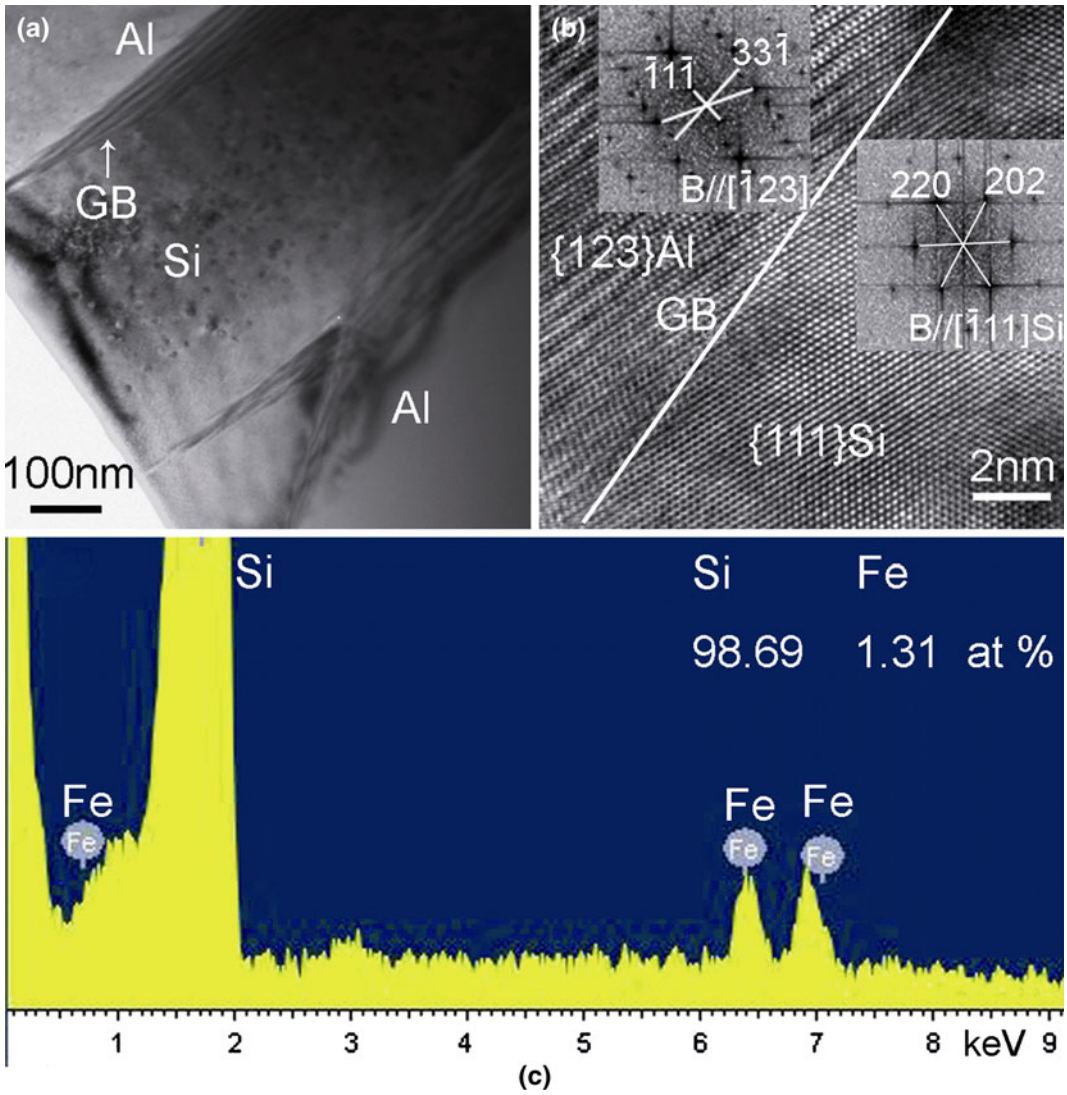

Fig. 8—TEM bright field image of a plate-shaped Si phase (*a*), high-resolution TEM image of a grain boundary (*b*) in commercial purity Al-5Si-6100 ppm Yb alloy. (B//$\langle 111 \rangle_{Si}$). EDX analysis (*c*) was taken from the Si particle.

completely consumed by Na, which can be easily adapted for YbP phase as follows:

$$C_{Yb} = \left(\frac{w_{Yb}}{w_P}\right) C_P$$

where w_{Yb} is atomic weight of Yb (173.05 g)[29] and w_p is atomic weight of P (30.97 g),[29] C_{Yb} is concentration of Yb, and C_P is concentration of P, respectively. After simplification this gives a relation $C_{Yb} \approx 5.59 C_P$ to form YbP phase. Similarly, a relation $C_{Al} \approx 0.87 C_P$ can be obtained to form AlP compounds. Clearly, the formation of YbP consumes much more P than that consumed for the formation of AlP, by a factor of 6.43. It is important to point out that the lack of AlP only results in an increased nucleation undercooling and thereby refinement of eutectic Si structure, but cannot explain the modification caused by twins.

C. *Refinement or Modification of Eutectic Si*

A refined plate-like eutectic structure was achieved when the Yb content was increased to 6100 ppm (Figures 3(d) and (e)). Even with a higher Yb addition (up to 13400 ppm Yb in Al-10Si alloy, and 10000 ppm Yb in Al-7.5Si-0.45Mg alloy) reported by another study,[11] only refined Si can be achieved, compared with the modification of 200 ppm Na addition. Similar refinement of eutectic Si caused by the addition of other rare earth elements (*i.e.*, Sc,[6] La, Ce[7], *etc.*) was also reported, and often regarded as modification.[4,5] One particular question that arises is whether this "declared modification" caused by the addition of rare earth elements is equal to the modification caused by the addition of Sr and Na, showing significant twins in Si. It is generally accepted that modification of eutectic Si can be directly related to the depression of the eutectic growth temperature. In this study, a reduction of

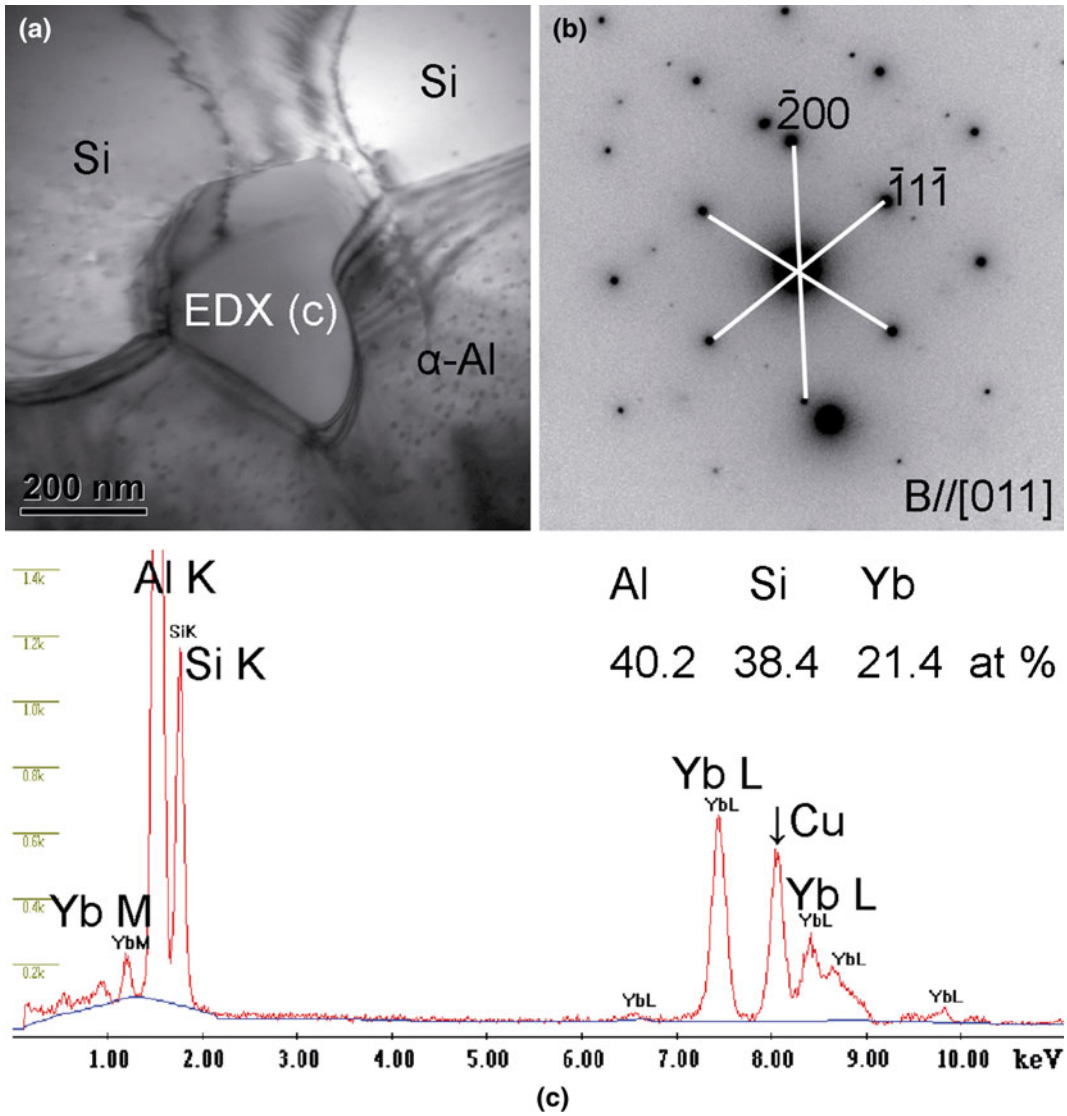

Fig. 9—TEM bright field image (*a*) and corresponding SADP (*b*), EDX analysis (*c*) of the Al_2Si_2Yb phase in commercial purity Al-5Si-6100 ppm Yb alloy. The presence of Cu peak is due to the TEM holder.

Table III. Crystallographic Data for Some Selected Phases

No.	Phase	Crystal Structure	Lattice Parameter (nm)	Disregistry (δ) (Percent)
1	Al	cubic	$a = 0.40491$	25 when $(Al)_S$
2	Si	cubic	$a = 0.5421$	
3	Al_2Si_2Sr	hexagonal	$a = 0.41872$, $c = 0.7427$	23 when $(Al_2Si_2Sr)_S$
4	Al_2Si_2Yb	hexagonal	$a = 0.414482$, $c = 0.68927$	23 when $Al_2Si_2Yb)_S$
5	AlP	cubic	$a = 0.5431$	<1 when $(AlP)_S$
6	YbP	cubic	$a = 0.5554$	<1 when $(YbP)_S$
7	$AlPO_4$	hexagonal	$a = 0.4390$, $c = 1.0940$	19 when $(AlPO_4)_S$
8	Al_2O_3	hexagonal	$a = 0.4785$, $c = 1.2991$	>19 when $(Al_2O_3)_S$

eutectic growth temperature [T_G, 836.5 K (563.5 °C) for 2000 ppm Yb addition (Alloy E), and 833 K (560 °C) for 6100 ppm Yb addition (Alloy F)] was observed. However, only refined smaller Si was achieved. This strongly indicated that no direct relationship can be expected between the Si morphology and the depression of eutectic growth temperature. In contrast, growth undercooling ($T_{eq} - T_G$) and recalescence ($T_G - T_{Min}$) of the eutectic arrest shows a good prediction to the refinement effect of Yb addition. Lower growth undercooling [8.4 K (8.4 °C) for alloy A] and recalescence [1.1 K (1.1 °C) for alloy A] observed at Yb less

Table IV. Enthalpies and Gibbs Energies of Formation of Different Phosphides (1 mol P)

Phosphide Compounds	Enthalpy, ΔH^0_{298} (kJ mol^{-1})	Gibbs Energy, ΔG^0_{298} (J mol^{-1} K^{-1})
AlP	−111.66	−113.48
SiP	−38.84	−38.44
FeP	−95.22	−97.28
CrP	−120.60	−120.74
MnP	−119.67	−117.92
Ba_3P_2	−280.77	−278.5
Ca_3P_2	−249.87	−246.86
Sr_3P_2	−317.5	—
Na_3P	−202	—
ScP	−347.35	−345.39
LaP	−363.72	−359.88
YP	−374.83	−375.86
YbP	—	—

than 2000 ppm, results in a very coarse and flake-like eutectic Si structure. Higher growth undercooling [14.0 K (14.0 °C) for alloy F and 14.7 K (14.7 °C) for alloy G], and recalescence [5.4 K (5.4 °C) for alloy F and 5.8 K (5.8 °C) for alloy G] leads to a refined plate-like eutectic structure. In the current study, the formation of Al_2Si_2Yb phase (Figures 4 and 9) consumes most of Yb. Moreover, the suggested formation of thermodynamically stable YbP phase is also expected to partially consume P, depleting the AlP phase. However, the YbP did not act as a potent nucleation sites for Si. Thus, increasing Yb addition results in a refined microstructure, especially for the high-purity Al-5Si-6100 ppm Yb alloy (alloy G). Although, the recalescence ($T_G - T_{Min}$) is also denoted as undercooling, however, undercooling is more commonly used to describe the drop of nucleation temperature ($T_{eq} - T_N$). As suggested by Dahle and co-workers,[5] the recalescence is also thought to be a good description of eutectic arrest.

The partitioning behavior and the solute redistribution during solidification process are of great importance to elucidate the refinement or modification mechanism. Yb has a very limited solubility in Al. The maximum Yb solid-solubility in α-Al measured by atom probe tomography was found to be 0.0248 ± 0.0007 (at. pct) at 898 K (625 °C).[35] The diffusivity of Yb in Al and the Al/Al_3Yb interfacial free energies at 573 K (300 °C) were also measured to be $(6 \pm 2) \times 10^{-17}$ m^2 s^{-1} and 0.6 ± 0.3 J m^{-2}, respectively.[35] During the solidification process, Yb and Si elements were rejected to the front of the advancing solid-liquid interface. An undercooling was established, as shown in Figure 1 and Table II, which restricts the growth of eutectic Si and thus refines the eutectic Si structure. This refinement mechanism caused by undercooling is different from the well-known IIT and TPRE modification mechanisms, because, unlike Sr and Eu, Yb does not concentrate in the eutectic Si and show significant twins at conventional casting rate. Given that the modification is mainly focused on the morphology change from plate-like to fibrous, we therefore, prefer to describe the effect of Yb as well as other similar rare earth elements (*i.e.*, Y, Ce, and Sc) on eutectic Si as a refinement, rather than a modification.

Last, but definitely not the least, the cooling rate is also of great importance to the refinement or modification of eutectic Si. Higher cooing rates, such as in chill casting and melting spinning in comparison to the sand casting, can extend the solid solubility of Yb in α-Al matrix,[36] resulting in a solute redistribution of Yb, force twinning, and thus causing a modification effect to occur. Further research on higher cooling rates is required to elucidate the effect of different cooling rates on refinement or modification of eutectic Si in Al-Si-based alloys with Yb additions.

V. CONCLUSIONS

Thermal analysis and multiscale microstructure characterization techniques have been employed to investigate the effect of Yb additions (up to 6100 ppm) on the eutectic Si in a series of Al-5 wt pct Si alloys. The following conclusions can be drawn:

1. The addition of Yb was found to cause no modification effect to a fibrous morphology involving Si twinning; however, a refined plate-like eutectic structure was observed.
2. The Al_2Si_2Yb phase was observed at more than 1000 ppm Yb addition level. Within the eutectic Al and Si phases, the Al_2Si_2Yb phase was found as a precipitation from the remained liquid. No Yb was detected in the α-Al matrix or plate-like Si particle, even with Yb addition of up to 6100 ppm. The absence of Yb element inside the eutectic Si may partly explain why no clear Si twinning was observed along $\{111\}_{Si}$ planes in the eutectic Si particles.
3. The formation of the thermodynamic stable YbP phases is also proposed to deteriorate the AlP potency in Al alloys.
4. This investigation highlights to distinguish modifications associated with the ever present P in Al alloy. In this context, modification is defined as a transition from faceted to fibrous involving Si twinning, while a reduction of the Si size is termed refinement.

ACKNOWLEDGMENTS

Jiehua Li is grateful to Prof. Gerhard Dehm for allowing him to access TEM, and Prof. Jozef Keckes for his help on XRD analysis at the Erich Schmid Institute of Materials Science of the Austrian Academy of Science.

REFERENCES

1. A. Pacz: U.S Patent No. 1387900, 1921.
2. S.-Z. Lu and A. Hellawell: *Metall. Trans. A*, 1987, vol. 18A, pp. 1721–33.
3. B. Li, H.W. Wang, J.C. Jie, and Z.J. Wei: *J. Alloys Compd.*, 2011, vol. 509, pp. 3387–92.

4. K. Nogita, A. Knuutinen, S.D. McDonald, and A.K. Dahle: *J. Light Met.*, 2001, vol. 1, pp. 219–28.
5. A. Knuutinen, K. Nogita, S.D. McDonald, and A.K. Dahle: *J. Light Met.*, 2001, vol. 1, pp. 229–40.
6. W. Prukkanon, N. Srisukhumbowornchai, and C. Limmaneevichitr: *J. Alloys Compd.*, 2009, vol. 477, pp. 454–60.
7. Y.C. Tsai, C.Y. Chou, R.R. Jeng, S.L. Lee, and C.K. Lin: *Int. J. Cast Metal. Res.*, 2011, vol. 24, pp. 83–87.
8. Q.Y. Zhang, C.G. Zheng, and W.S. Han: *Acta Metall. Sin.*, 1981, vol. 17, pp. 130–36.
9. M. Timpel, N. Wanderka, R. Schlesiger, T. Yamamoto, N. Lazarev, D. Isheim, G. Schmitz, S. Matsumura, and J. Banhart: *Acta Mater.*, 2012, vol. 60, pp. 3920–28.
10. K. Nogita, H. Yasuda, K. Yoshida, K. Uesugi, A. Takeuchi, Y. Suzuki, and A.K. Dahle: *Scripta Mater.*, 2006, vol. 55, pp. 787–90.
11. K. Nogita, H. Yasuda, M. Yoshiya, S.D. McDonald, K. Uesugi, A. Takeuchi, and Y. Suzuki: *J. Alloys Compd.*, 2010, vol. 489, pp. 415–20.
12. M. Faraji and L. Katgerman: *Micron.*, 2010, vol. 41, pp. 554–59.
13. M. Zarif, B. McKay, and P. Schumacher: *Metall. Mater. Trans. A*, 2011, vol. 42A, pp. 1684–91.
14. X. Jian, T.T. Meek, and Q. Han: *Scripta Mater.*, 2006, vol. 64, pp. 893–96.
15. J.B. Yu, Z.M. Ren, and K. Deng: *Acta Metall. Sin.*, 2011, vol. 24, pp. 301–08.
16. A.G.C. Gwyer and H.W.L. Philips: *J. Inst. Met.*, 1926, vol. 36, p. 283.
17. C.E. Ransely and H. Neufeld: *J. Inst. Met.*, 1950–1951, vol. 78, p. 25.
18. R.C. Plumb and J.E. Lewis: *J. Inst. Met.*, 1957–1958, vol. 86, pp. 393–400.
19. A. Hellawell: *The Growth and Structure of Eutectics with Silicon and Germanium*, Pergamon Press, Great Britain, 1970, p. 72.
20. L. Guillet: *Rev. Met.*, 1922, vol. 19, p. 303.
21. S.C. Flood and J.D. Hunt: *Metal Science*, 1981, vol. 15, pp. 287–94.
22. C.R. Ho and B. Cantor: *J. Mater. Sci.*, 1995, vol. 20, pp. 1912–20.
23. J.H. Li, M. Zarif, G. Dehm, and P. Schumacher: *Philos. Mag.* doi: 10.1080/14786435.2012.687840.
24. R.S. Wanger: *Acta Metall.*, 1960, vol. 8, p. 57.
25. R.D. Hamilton and R.G. Seidensticker: *J. Appl. Phys.*, 1960, vol. 31, p. 1165.
26. A.L. Greer: *Philos. Trans. R. Soc. Lond. A*, 2003, vol. 361, pp. 479–95.
27. S. Bobev, P.H. Tobash, V. Fritsch, J.D. Thompson, M.F. Hundley, J.L. Sarrao, and Z. Fisk: *J. Solid State Chem.*, 2005, vol. 178, pp. 2091–2103.
28. L. Heusler and W. Schneider: *J. Light Metal.*, 2002, vol. 2, pp. 17–26.
29. E.A. Brandes and C.J. Smithells, *Metals Reference Handbook*, 6th ed., Butterworths Publishing Company, London, 1983, pp. 6–29.
30. D. Turnbull and B. Vonnegut: *Ind. Eng. Chem.*, 1952, vol. 44, p. 1292.
31. P. Villars and L.D. Calvert, eds.: *Pearsons Handbook of Crystallographic Data of Intermetallic Phase*, vols. 1–3, American Society for Metals, Metal Park, 1985, p. 3258.
32. H.R. Ott, H. Rudigier, and F. Hulliger: *Solid State Commum.*, 1985, vol. 55, p. 113.
33. M.E. Schlesinger: *Chem. Rev.*, 2002, vol. 102, pp. 4267–4301.
34. O. Knacke, O. Kubaschewski, and K. Hesselmann: *J. Phys. Chem. Ref. Data*, 1982, vol. 11, pp. 2–279.
35. M.E. van Dalen, R.A. Karnesky, J.R. Cabotaje, D.C. Dunand, and D.N. Seidman: *Acta Mater.*, 2009, vol. 57, pp. 4081–89.
36. Y.T. Ning, X.M. Zhou, and H. Dai: *Acta Metall. Sin.*, 1992, vol. 5, pp. 327–33.